September 2004

Magnetic impurities in conducting oxides. II. $(Sr_{1-x}La_x)(Ru_{1-x}Co_x)O_3$ system

Alexander Mamchik
University of Pennsylvania

Wotjek Dmowski
University of Tennessee

Takeshi Egami
University of Tennessee

I-Wei Chen
University of Pennsylvania, iweichen@seas.upenn.edu

Magnetic impurities in conducting oxides. II. $(Sr_{1-x}La_x)(Ru_{1-x}Co_x)O_3$ system

Abstract

The perovskite solid solution between ferromagnetic $SrRuO_3$ and antiferromagnetic $LaCoO_3$ is studied and its structural, electronic, and magnetic properties are compared with $(Sr_{1-x}La_x)(Ru_{1-x}Fe_x)O_3$. The lower $3d$ energy levels of Co^{3+} cause a local charge transfer from $4d$ Ru^{4+}, a reaction that has the novel feature of being sensitive to the local atomic structure such as cation order. Despite such a complication, Co, like Fe, spin-polarizes the itinerant electrons in $SrRuO_3$ to form a large local magnetic moment that is switchable at high fields. In the spin glass regime when Anderson localization dominates, a large negative magnetoresistance emerges as a result of spin polarization of mobile electronic carriers that occupy states beyond the mobility edge. A phenomenological model predicting an inverse relation between magnetoresistance and saturation magnetization is proposed to explain the composition dependence of magnetoresistance for both $(Sr_{1-x}La_x)(Ru_{1-x}CO_x)O_3$ and $(Sr_{1-x}La_x)(Ru_{1-x}Fe_x)O_3$ systems.

Magnetic impurities in conducting oxides. II. $(Sr_{1-x}La_x)(Ru_{1-x}Co_x)O_3$ system

A. Mamchik,[1] W. Dmowski,[2] T. Egami,[2] and I-Wei Chen[1,*]

[1]*Department of Materials Science and Engineering, University of Pennsylvania, Philadelphia, Pennsylvania 19104-6272, USA*
[2]*Department of Materials Science/Physics and Astronomy, University of Tennessee, Knoxville, Tennessee 37996-1508, USA*

The perovskite solid solution between ferromagnetic $SrRuO_3$ and antiferromagnetic $LaCoO_3$ is studied and its structural, electronic, and magnetic properties are compared with $(Sr_{1-x}La_x)(Ru_{1-x}Fe_x)O_3$. The lower $3d$ energy levels of Co^{3+} cause a local charge transfer from $4d$ Ru^{4+}, a reaction that has the novel feature of being sensitive to the local atomic structure such as cation order. Despite such a complication, Co, like Fe, spin-polarizes the itinerant electrons in $SrRuO_3$ to form a large local magnetic moment that is switchable at high fields. In the spin glass regime when Anderson localization dominates, a large negative magnetoresistance emerges as a result of spin polarization of mobile electronic carriers that occupy states beyond the mobility edge. A phenomenological model predicting an inverse relation between magnetoresistance and saturation magnetization is proposed to explain the composition dependence of magnetoresistance for both $(Sr_{1-x}La_x)(Ru_{1-x}CO_x)O_3$ and $(Sr_{1-x}La_x)(Ru_{1-x}Fe_x)O_3$ systems.

I. INTRODUCTION

Perovskite $SrRuO_3$ is a Stoner ferromagnet despite its relatively low (bad metallic) conductivity.[1] The Stoner criterion is satisfied because of high density of states at the Fermi level that critically enhances the electron magnetic susceptibility. Metals that possess high-density of states at the Fermi levels can form giant localized magnetic moments around magnetic impurities that polarize the neighboring itinerant electrons. This has been well documented in alloys of palladium, which has the highest density of states among $4d$ metals.[2,3] The first evidence for this phenomenon in oxides was found in our previous study (hereafter referred to as **I**) on $SrRuO_3$ substituted with $LaFeO_3$, in which Fe^{3+} cations induce an enhanced saturation moment in the host $SrRuO_3$ matrix.[4] Unlike Pd alloys, however, $SrRuO_3$ suffers from Anderson localization at high Fe concentration, resulting in a metal-to-semiconductor transition.[4,5] Nevertheless, by aligning the spin-polarized electron atmospheres around Fe^{3+} under a field, a large negative magnetoresistance (MR) emerges at low temperatures in $(Sr_{1-x}La_x)(Ru_{1-x}Fe_x)O_3$ semiconductor.[4,5] The presence of Fe^{3+} also gives rise to similarly large negative MR in paramagnetic conducting $CaRuO_3$ and Sr_2RuO_4, presumably because they are already on the verge of Stoner ferromagnetism.[5] In this study, we have investigated a closely related system, $SrRuO_3$ partially substituted with $LaCoO_3$ to further establish this mechanism in Stoner ferromagnetic conducting oxides.

Like Fe^{3+}, Co^{3+} provides $3d$ electron energy levels that are in the vicinity of the Fermi level of $SrRuO_3$. This is an important prerequisite for forming a large localized magnetic moment according to Anderson, Wolff, and Clogston, who treated localized moments as virtual bound states that arise by resonance.[6–8] Therefore, if our hypothesis of electron polarization is correct, then very similar behavior, including enhanced saturation magnetization and a large negative MR, should also be observed in Co-substituted $SrRuO_3$. On the other hand, Co^{3+} has somewhat lower energy

levels compared to Fe^{3+}, and there have been numerous reports of the complicated transitions between the various electronic states of Co, including high-spin Co^{2+}, Co^{3+}, and Co^{4+}, intermediate-spin Co^{3+} and Co^{4+}, and low-spin Co^{3+} and Co^{4+}.[9–13] Therefore, it is by no mean obvious *a priori* that $(Sr_{1-x}La_x)(Ru_{1-x}Co_x)O_3$ should behave like $(Sr_{1-x}La_x)(Ru_{1-x}Fe_x)O_3$. A previous investigation of $SrRu_{0.9}Co_{0.1}O_3$ did suggest an enhanced saturation magnetization, but the negative MR in this solid solution was limited to the vicinity of Curie temperature and could not be attributed to the localized moments at Co.[14] A negative MR was also observed in $La_{0.5}Sr_{0.5}Co_{0.9}Ru_{0.1}O_3$,[15] however, this is related to the negative MR in $La_{0.5}Sr_{0.5}CoO_3$ caused by the mixed valency of Co^{3+}/Co^{4+}.[16] In this study, we will show that, despite the complication of electronic transitions between high-spin Co^{3+} and Co^{2+}, which cause ordering and clustering among Ru and Co,[17] the basic phenomena of localized moment formation and large negative MR remain intact in the $(Sr_{1-x}La_x)(Ru_{1-x}Co_x)O_3$ system.

II. EXPERIMENTAL PROCEDURES

Ceramic samples of composition $(Sr_{1-x}La_x)(Ru_{1-x}Co_x)O_3$ $(0 \leq x \leq 0.5)$ were prepared by the solution polymerization technique described elsewhere.[18] The procedure started with the thermal decomposition of a polymeric gel made from mixing RuO_2, nitrates of Sr, La and Co, and poly(ethyleneglycol). After thermal decomposition, pressed powders were sintered at temperatures between 1200°C and 1300°C. During sintering, pellets were packed in an excess amount of $SuRuO_3$ powder to prevent Ru volatilization. After sintering, the surface layers of the pellets were removed before further characterization.

X-ray powder diffraction (XRD) was conducted using Cu $K\alpha$ radiation with Si powder added as an internal standard. Crystal structure refinement was conducted for the sample with $x=0.2$ using powder diffraction data (0.70309 Å wavelength) collected at the X−7A beamline at the National

TABLE I. Summary of structure and magnetic data in $Sr_{1-x}La_xRu_{1-x}Co_xO_3$. Standard deviation of temperature (T) is estimated to be $+/-1$ K, taking into account the instrumentation precision (0.1 K), cooling/heating rate (2% min), and sampling interval (1–3 K) for data that were then smoothed by interpolation. μ_{sat} is the average moment, in Bohr magneton, of each B-site cation, calculated from $M(9\text{ T})$ at 10 K using the conversion factor of 5584.8 emu/mol$=1\mu_B$.

x	0.0	0.1	0.2	0.3	0.4 ord	0.4 disord	0.5 ord	0.5 disord
a(Å)	5.5738(4)	5.5758(4)	5.5812(4)	5.5843(3)	5.5892(8)	5.5854(8)	5.5869(3)	5.5741(6)
b(Å)	7.8524(5)	7.8585(5)	7.8626(8)	7.8679(6)	7.865(26)	7.8660(2)	7.8740(3)	7.8678(5)
c(Å)	5.5353(6)	5.5408(7)	5.5454(4)	5.5470(5)	5.560(11)	5.5565(8)	5.5611(5)	5.5613(2)
β(°)	90	90	90.01(1)	90.026(5)	90.05(2)	90.026(1)	90.076(4)	90.263(9)
V(Å^3)	242.265(1)	242.781(2)	243.346(1)	243.719(1)	244.419(4)	244.123(2)	244.639(1)	243.896(1)
T_C(K)	161	102	54					
T_f(K)				56.5	48.5	48	53	46
θ_{CW}(K)	162.7(5)	121.0(4)	69.7(4)	1.1(8)	−33.1(6)	−36(1)	−56(1)	−56(1)
$\mu_{eff}(\mu_B$/mol)	2.608(3)	3.244(1)	3.902(3)	4.34(2)	4.61(1)	4.37(4)	4.72(3)	4.44(5)
$\mu_{sat}(\mu_B$/mol)	1.3804(1)	1.5771(1)	1.0835(2)	0.4727(2)	0.4315(1)	0.3790(1)	0.3189(2)	0.3351(1)

Synchrotron Light Source (NSLS), Brookhaven National Laboratory. These XRD data were collected at room temperature. In addition, diffraction data at 10 K were collected using time-of-flight (TOF) neutron diffraction at GPPD station at IPNS at Argonne National Laboratory.

The valence state of Ru in the compounds was determined by synchrotron x-ray absorption near edge structure (XANES) on the Ru L_{III} edge at the X19B beamline at NSLS. The spectra were collected in the fluorescence mode using a solid-state detector. Measurements were performed using a step width of 0.1 eV and a counting time of 1 s per datum point in the energy range of 2820–2850 eV selected by a Si(111) monochromator. The K edge of elemental S (2472 eV) was used for photon energy calibration before measurements.

Four-point resistivity and magnetic measurements were performed in a physical property measurement system (PPMS; Quantum Design) in the temperature range of 5–350 K and under a magnetic field up to 9 T. The field direction is perpendicular to the long axis of the specimen for resistivity measurements and along the long axis for magnetic measurements. The magnetocrystalline anisotropy was not studied because of the absence of texture in the ceramics and in view of our previous finding of insignificant magnetoresistance anisotropy in epitaxial thin films. The MR value was calculated with reference to the zero field resistance taken after a complete field cycle to remove the effect of shape anisotropy and irreversible changes during the first cycle. Other details of the experiments have been described elsewhere.[4,18]

III. RESULTS

A. X-ray and neutron diffraction data

The XRD of all the samples used in this study had a single-phase pattern with all the reflections identifiable with those of perovskite lattice. (See Table I.) It is known that perovskite-based structures are also adopted by the end-member compounds, space group $Pnma$ for SrRuO$_3$ and $R\bar{3}c$ for LaCoO$_3$.[13,19,20] The intermediate compound, $Sr_{1/2}La_{1/2}Ru_{1/2}Co_{1/2}O_3$, however, is monoclinic according to Kim and Battle,[17] with the B-site cations, Ru and Co, 1:1 ordered in the NaCl pattern in the space group $P2_1/n$ (No. 14). Direct evidence for B-site ordering was found in our study for $x=0.4$ and 0.5, most prominently by the presence of the (1/2 1/2 1/2) superlattice reflection in the XRD pattern. This is consistent with a doubling of the unit cell along the [111] pseudocubic direction and the 1:1 (B-site) order of the NaCl type.

For the $x=0.5$ samples, the order/disorder transition occurs between 1500°C and 1600°C as illustrated in Fig. 1 which shows the XRD patterns of several samples heat treated at various temperatures from 1300°C to 1600°C. The figure also illustrates that the disordered sample (air-quenched from 1600°C) can be ordered again by reannealing at 1200°C. The relative peak intensity of the superlattice
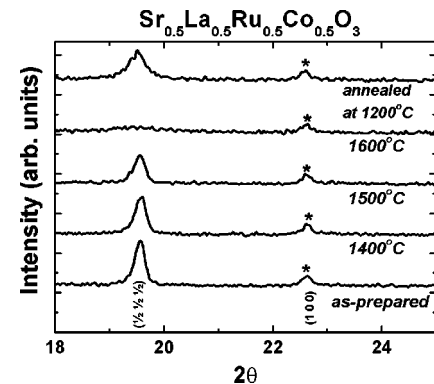

FIG. 1. Powder XRD patterns of $Sr_{0.5}La_{0.5}Ru_{0.5}O_3$ samples, initially sintered at 1300°C for 12 h. Additional samples were later annealed at 1400°C, 1500°C, or 1600°C for 10 min, followed by quenching. One sample was reannealed at 1200°C for 12 h after quenching from 1600°C. The superlattice reflection $\left(\frac{1}{2}\frac{1}{2}\frac{1}{2}\right)$ at $2\theta \sim 19.5°$ and the fundamental reflection (100) at $2\theta \sim 22.6°$ are both labeled in the pseudocubic notation.

TABLE II. Structure parameters for $Sr_{0.8}La_{0.2}Ru_{0.8}Co_{0.2}O_3$ at 10 K from time-of-flight neutron diffraction data. Space group: $P21/n(\#14, P12_1/n1)$. Unique b axis, origin at 1. $a=5.5714(1)$Å, $b=5.5368(1)$Å, $c=7.8452(2)$Å, $\beta=90.008(2)°$, $V=242.003(5)$Å^3. The refinement was performed using the GSAS software package, (Ref. 37), and it converged with values $R_p=6.70\%$ and $wR_p =10.58\%$.

Atom	Site	x	y	z	U_{iso}(Å^2)	n
Sr	4e	0.0041(4)	0.166(6)	0.2439(12)	0.0042(3)	0.8
La	4e	0.0041(4)	0.0166(3)	0.2439(12)	0.0042(3)	0.2
Co	2d	1/2	0	1/2	0.0024(2)	0.2
Ru	2d	1/2	0	1/2	0.0024(2)	0.8
Co	2c	1/2	0	0	0.0024(2)	0.2
Ru	2c	1/2	0	0	0.0024(2)	0.8
O$_1$	4e	0.2790(1)	0.2814(5)	0.0312(4)	0.0062(7)	1
O$_2$	4e	0.2279(14)	−0.2284(2)	0.0267(5)	0.0042(6)	1
O$_3$	4e	−0.0564(3)	0.4931(5)	0.2397(20)	0.0088(7)	1

reflection with reference to the fundamental structure reflection, $I_{(1/2\ 1/2\ 1/2)}/I_{(100)}$, was compared with the calculated ratio to estimate the degree of order (the relative intensity being proportional to the squared degree of order). It ranges from 78% in the sample sintered at 1300°C or reannealed at 1200°C to 42% in the sample quenched from 1600°C. For brevity, the two samples will be referred to as "ordered" and "disordered" samples, respectively, even though they are neither completely ordered nor disordered. The ordering temperature for the $x=0.4$ sample was similarly determined to be between 1300°C and 1400°C. Obviously, the 1:1 ordered structure was less favored because of off-stoichiometry in the $x=0.4$ composition.

Although ordering occurs only in the $x=0.4$ and 0.5 samples, which adopt the monoclinic $P2_1/n$ structure, a disordered monoclinic structure also fits the XRD data of the $x=0.2$ and 0.3 samples. The fitting parameters for the monoclinic unit cell are tabulated in Table I, which shows that monoclinic distortion begins at about $x=0.2$. A further verification of the assignment of the cation-disordered monoclinic space group was obtained for the $x=0.2$ sample by Rietveld structure refinement using data of neutron powder diffraction. The results are shown in Table II in terms of a $P2_1/n$ structure that consists of a random placement of Sr and La on the A site (4e) as well as a random placement of Ru and Co on the B sites (both 2c and 2d), all at the nominal composition ($x=0.2$). The average $B-O-B$ angle determined is 162.07°, which is similar to that (163°) in SrRuO$_3$.

The lattice parameters in Table I are plotted in Fig. 2. There appears to be a change at $x=0.4$ regardless of the state of order. The unit cell volume computed from these data gradually increases with x, even though the cell volume of LaCoO$_3$ (224.0 Å^3) is much smaller than that of SrRuO$_3$ (242.26 Å^3).[13,19,20] This indicates that the radius of Co in our samples is larger than that in LaCoO$_3$, where Co is in the low-spin state of Co^{3+} with a radius of 0.545 Å. Therefore, Co in our samples is likely to be in the high-spin state, as either Co^{3+} (0.61 Å) or Co^{2+} (0.745 Å).[21] Also note that
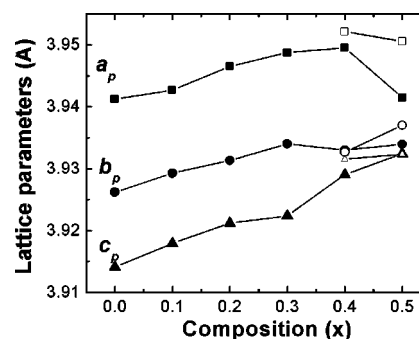

FIG. 2. Monoclinic lattice parameters, in pseudocubic representation, of the disordered and ordered samples as a function of composition. Ordered samples in open symbols.

the cell volume is larger in the ordered samples for the reason that will become clear below.

B. XANES

Previously, Kim and Battle speculated that Ru^{5+} and Co^{2+} existed in the ordered $Sr_{1/2}La_{1/2}Ru_{1/2}Co_{1/2}O_3$ compound they prepared.[17] This speculation was based on the Mössbauer study of a similar double perovskite, $Ba_{1/2}La_{1/2}Ru_{1/2}Co_{1/2}O_3$.[22] The proposition is attractive since it would provide a strong justification for the observed B-site ordering, inasmuch as the charge and size contrast is much larger in the (Ru^{5+},Co^{2+}) pair than in the (Ru^{4+},Co^{3+}) pair. Ru^{4+} (0.62 Å) is rather similar in size to high-spin Co^{3+}(0.61 Å), but high-spin Co^{2+}(0.745 Å) is much larger than Ru^{5+}(0.565 Å).[21] We have obtained direct evidence for the existence of Ru^{5+} in the $Sr_{1-x}La_xRu_{1-x}Co_xO_3$ series from Ru L_{III}-edge XANES, shown in Fig. 3, which also includes the spectra of the following model compounds: CaRuO$_3$ containing Ru^{4+}; and SrY$_{1/2}$Ru$_{1/2}$O$_3$, an ordered double perovskite containing Ru^{5+}. Our previous study of $Sr_{1-x}La_xRu_{1-x}Fe_xO_3$ has identified the two peaks in the Ru L_{III}-edge XANES with the $2p \rightarrow t_{2g}$ and $2p \rightarrow e_g$ transitions.[4] These transitions shift to a higher energy and are more separated when Ru^{5+} replaces Ru^{4+}, because Ru^{5+} has
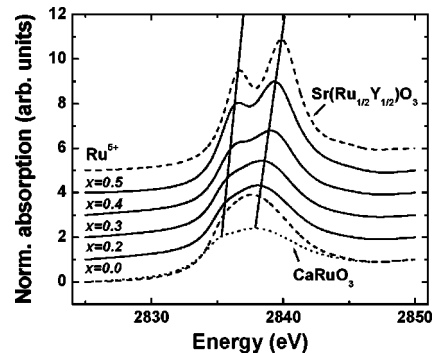

FIG. 3. Ru L_{III}-edge XANES spectra of $Sr_{1-x}La_xRu_{1-x}Co_xO_3$ samples. Also included are the spectra of CaRuO$_3$ and (SrRu$_{1/2}$Y$_{1/2}$)O$_3$. All the samples are as-sintered, therefore ordered in the case of $x=0.4$ and 0.5. Lines indicating peak positions are an aid to eyes.
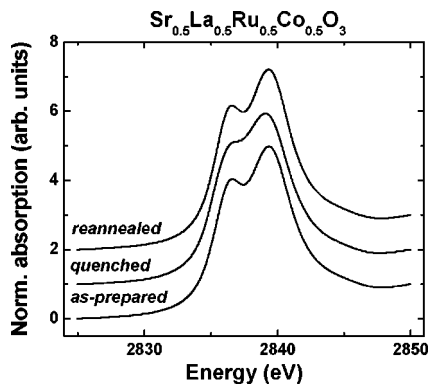
FIG. 4. Ru L_{III}-edge XANES spectra of three $Sr_{0.5}La_{0.5}Ru_{0.5}Co_{0.5}O_3$ samples, in the as-sintered (ordered) state, the 1600°C quenched (disordered) state, and the 1200°C reannealed (ordered) state.

lower core-electron energy levels and a stronger ligand field. It is clear that, with increasing x, the spectra in Fig. 3 progressively shift from that of Ru^{4+} (as in $CaRuO_3$) to that of Ru^{5+} (as in $SrY_{1/2}Ru_{1/2}O_3$). In contrast, in the $Sr_{1-x}La_xRu_{1-x}Fe_xO_3$ series, there is no such shift and only Ru^{4+} exists.[4]

Importantly, we have also found that ordering exerts a strong effect on the XANES spectra. Figure 4 shows the spectra of three $Sr_{1/2}La_{1/2}Ru_{1/2}Co_{1/2}O_3$ samples, in the as-sintered (ordered) state, the 1600°C quenched (disordered) state, and the 1200°C reannealed (ordered) state. The disordered sample show less Ru^{5+} features than the two ordered samples, which have indistinguishable spectra. These results indicate that the charge transfer from $Ru^{4+}:Co^{3+}$ to $Ru^{5+}:Co^{2+}$ is a short range reaction that is favored when Ru and Co are nearest neighbors to each other. In other words, the preferred charge states for the nearest-neighbor pairs are $Ru^{4+}-Ru^{4+}, Ru^{5+}-Co^{2+}$ and $Co^{3+}-Co^{3+}$. As noted above, the cell volumes (see Table I) of the ordered samples are larger than the disordered samples. This is now understandable since the sum of the ionic radii of Co^{2+} and Ru^{5+} exceeds that of Co^{3+} and Ru^{4+}. To our knowledge, this is the first time that a local-structure-dictated charge-transfer reaction is directly observed in a solid solution.

C. Induced moment

In the $Sr_{1-x}La_xRu_{1-x}Fe_xO_3$ series, Fe^{3+} substitution causes the destruction of itinerant ferromagnetism in the $SrRuO_3$ matrix. The competition of an antiferromagnetic $Fe^{3+}-Fe^{3+}$ interaction with itinerant ferromagnetism gives rise to a spin glass state that is preceded by a cluster glass state.[4,5] In addition, Fe^{3+} causes a magnetic polarization of the neighboring Ru electrons.[4] At low Fe concentrations, this results in a higher saturation moment for the solid solution than for $SrRuO_3$; at higher Fe concentrations, it participates in the cluster glass formation. As it will become clear below, the same phenomena were observed in the $Sr_{1-x}La_xRu_{1-x}Co_xO_3$ series, despite the complications of charge transfer between Ru and Co and their tendency to order.

The direct evidence that Co causes a polarization of the neighboring Ru electrons came from the measurement of dc
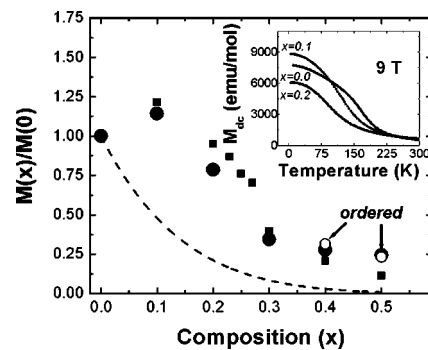

FIG. 5. Saturation magnetization at 10 K and 9 T to $Sr_{1-x}La_xRu_{1-x}Co_xO_3$ (solid circle for disordered and open circle for ordered) and $Sr_{1-x}La_xRu_{1-x}Fe_xO_3$ (solid square, data from **I**) as a function of x. Also shown in a broken curve is the $(1-x)^7$ prediction that describes the low field data of $Sr_{1-x}Ru_{1-x}Ti_xO_3$ and $Sr_{1-x}Ru_{1-x}Mg_xO_3$ in the literature (Refs. 24 and 25). The inset depicts the magnetization (M-T) curves at 9 T crossover between $x=0$ and 0.1 in the $Sr_{1-x}La_xRu_{1-x}Co_xO_3$ samples.

magnetization under a strong field. The saturation magnetization (taken at 9 T and 10 K) of $Sr_{1-x}La_xRu_{1-x}Co_xO_3$ is shown in Fig. 5, which also includes our previous data on $Sr_{1-x}La_xRu_{1-x}Fe_xO_3$ and the $x=0.5$ datum measured in this study. Both sets of data have a peak at $x=0.1$, and their overall magnitude is comparable. The peak is due to a crossover of the $x=0$ and $x=0.1$ $M(T)$ curves at low temperature and high field, as shown in the inset of Fig. 5. This crossover is also evident in the $M(H)$ hysteresis curves at 10 K, shown in Fig. 6. As in $Sr_{1-x}La_xRu_{1-x}Fe_xO_3$,[4] the crossover field of Fig. 5 is roughly proportional to the temperature; e.g., in the inset the crossover field is 9 T at 90 K, whereas in Fig. 6 it is 1.3 T at 10 K. Like $Fe^{3+}-Fe^{3+}$, the $Co^{3+}-Co^{3+}$ superexchange interaction is antiferromagnetic.[23] Therefore, the higher magnetization at $x=0.1$ cannot be due to cation clustering. Also, if the increased magnetization were due to the local moment of Co alone, then the switching field to align the moment would have been much higher because of magnetic anisotropy energy. Therefore, the extra, apparently switchable, magnetization most likely comes from large local moments induced by Co, which we believe are made of itinerant electrons locally polarized by Co. The fact that the
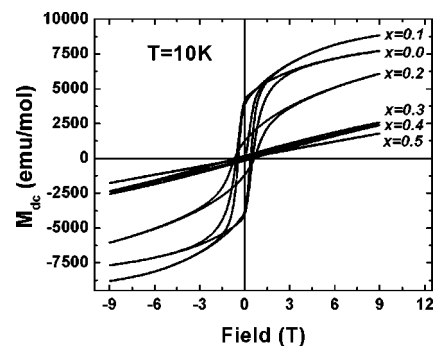

FIG. 6. Magnetization-field hysteresis curves at 10 K for disordered $Sr_{1-x}La_xRu_{1-x}Co_xO_3$ samples with different compositions. The crossover of saturation magnetization of $x=0.0$ and 0.1 curves can be seen.

magnitude and the shape of the saturation magnetization curves in Fig. 5 are similar for the Fe and the Co series suggests that their polarization mechanism is similar.

B-site substitution in $SrRuO_3$ has been reported to be extremely disruptive for the magnetic properties, depressing both T_c and saturation magnetization. For example, 10% of Ti or Mg substitution of Ru purportedly cause a suppression of T_c by about 50 K and a loss of magnetization of about 50% at low fields (typically 0.1 T)[24,25] This has been explained using the discontinuous magnetization model originally proposed by Jaccarino and Walker, which states that the alloy magnetism in an itinerant electron magnet depends on the composition of the nearest neighbors.[26] For both Ti and Mg substitution of the Ru sublattice, it was found that the magnetization follows a $(1-x)^7$ dependence, suggesting that a single substituted atom at any one of the (six) nearest neighbor sites around Ru is sufficiently disruptive to destroy the magnetic moment of Ru.[24,25] This dependence is plotted in Fig. 5 as a broken curve for reference. In addition, some disruptive effect, though less severe, has also been seen with *A*-site substitution.[24] Therefore, it might be expected that Fe and Co substitution, along with the accompanying *A*-site substitution by La, would too be disruptive. Contrary to this expectation, we found larger saturation moments at 10% Fe and Co addition. Therefore, for these substitutional cations, the strong magnetic polarization around them must more than compensate the disruptive effect they cause.

In Fig. 5 at small *x*, the saturation magnetization is initially lower in the $Sr_{1-x}La_xRu_{1-x}Co_xO_3$ series than in the $Sr_{1-x}La_xRu_{1-x}Fe_xO_3$ series, but the trend is reversed at $x=0.4$. (Both the ordered and disordered samples of $Sr_{0.6}La_{0.4}Ru_{0.6}Co_{0.4}O_3$ have significantly higher magnetization than $Sr_{0.6}La_{0.4}Ru_{0.6}Fe_{0.4}O_3$.) We can attribute this reversal to the ordering tendency of Ru and Co. At $x=0.4$, the probability of forming $Fe^{3+}-Fe^{3+}$ and $Co^{3+}-Co^{3+}$ pairs of nearest neighbors, both being antiferromagnetic, is very high at any given B site in a random solid solution. In Co solid solutions, however this probability should be much lower because Ru and Co tend to order, thus having a positive effect on overall magnetization. At $x=0.5$, where this contrast is the sharpest, the saturation magnetization of the Co solid solutions is twice the value of the Fe solid solutions.

D. Magnetic phase diagram

We determined the tentative magnetic phase diagram (inset in Fig. 7) for the disordered $Sr_{1-x}La_xRu_{1-x}Co_xO_3$ samples using the ac susceptibility data shown in Fig. 7. Although it lacks some of the details that were previously delineated for $Sr_{1-x}La_xRu_{1-x}Fe_xO_3$,[4] the two systems feature the same set of $T-x$ phase boundaries between magnetic states (paramagnetic, ferromagnetic, cluster glass and spin glass). Here the spin glass state was assigned by noting the susceptibility cusp at the freezing temperature T_f.[27] This assignment is also supported by the drastically lower magnitude (by up to 100 times) of spin glass susceptibility, compared to that of the ferromagnetic susceptibility at the Curie temperature (T_c). The cluster glass state was assigned to $Sr_{0.8}La_{0.2}Ru_{0.8}Co_{0.2}O_3$ by noting the following features: (a) the peak susceptibility is
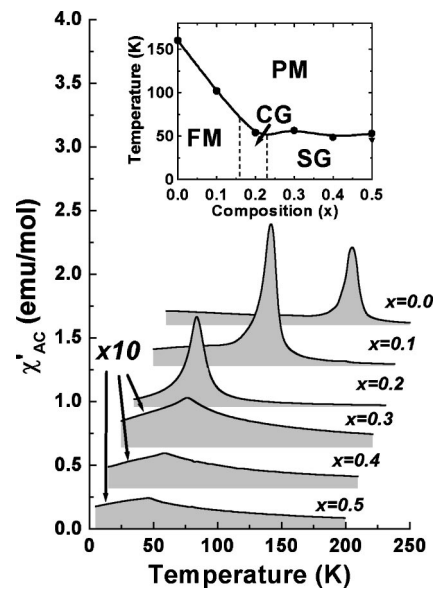

FIG. 7. ac 10 kHz magnetic susceptibility of disordered $Sr_{1-x}La_xRu_{1-x}Co_xO_3$ samples. Note that the data of $x=0.3$ and above are plotted at ten times the actual values. Inset: schematic magnetic phase diagram indicating regions for paramagnetic (PM), ferromagnetic (FM), cluster glass (CG), and spin glass (SG) states.

very high, and (b) the peak does not have a cusp shape but is highly frequency dependent, shifting to a higher temperature at a higher frequency.[27,28] See Fig. 8. Like the case of the $Sr_{1-x}La_xRu_{1-x}Fe_xO_3$ series (e.g., $Sr_{0.75}La_{0.25}Ru_{0.75}Co_{0.25}O_3$, which is a cluster glass),[4] $Sr_{0.8}La_{0.2}Ru_{0.8}Co_{0.2}O_3$ exhibits a large dc magnetization under a strong field, but the magnetization is nearly all lost once the field is removed, even at a temperature that is well below the peak susceptibility temperature (to which we also refer as T_c). This indicates that there are ferromagnetic clusters within the material but such clusters are weakly coupled with each other. Some details of these studies are given in the Appendix and further documented elsewhere.[18]

We next examine the effect of ordering and clustering on magnetic phases. Weak field magnetization of the (disordered) $x=0.3$ sample under field cooled (FC) and zero field cooled (ZFC) conditions are shown in Fig. 9(a). The ZFC curve has a sharp cusp typical for a spin glass. The FC curve has a higher magnetization at low temperature, which is common for a spin glass. Note the excess magnetization
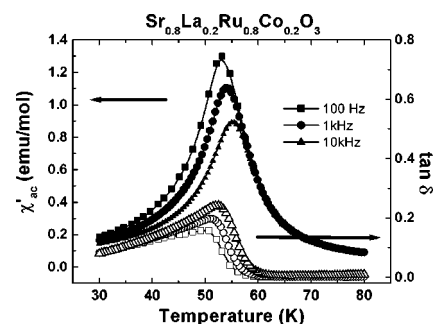

FIG. 8. ac susceptibility and tan δ of $Sr_{0.8}La_{0.2}Ru_{0.8}Co_{0.2}O_3$ at various frequencies.

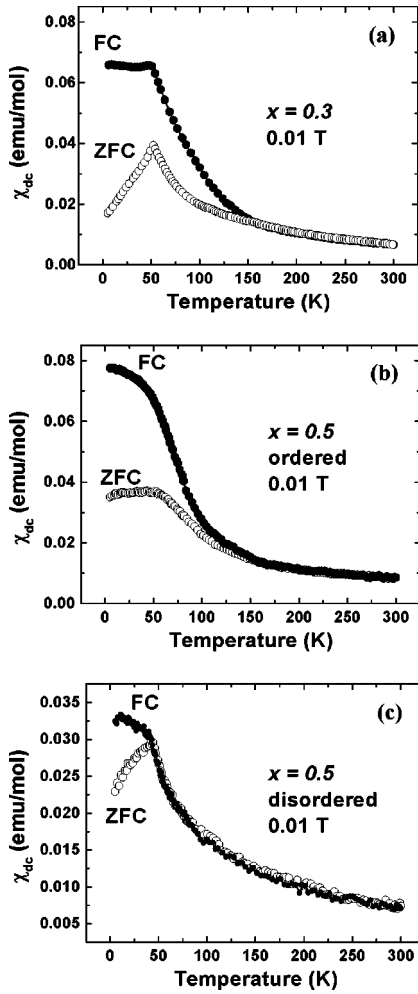FIG. 9. (a) Weak field magnetization of $Sr_{1-x}La_xRu_{1-x}Co_xO_3$ samples under FC and ZFC conditions (a) $Sr_{0.7}La_{0.3}Ru_{0.7}Co_{0.3}O_3$; (b) ordered $Sr_{0.5}La_{0.5}Ru_{0.5}Co_{0.5}O_3$; (c) disordered $Sr_{0.5}La_{0.5}Ru_{0.5}Co_{0.5}O_3$.

is no indication of a magnetic phase near 150 K except at a very low field (1 Oe) when a small shoulder appeared. The strong field magnetization curves do not indicate the presence of a ferromagnetic phase below 150 K either. Therefore, these $SrRuO_3$ clusters only dominate the weak field behavior when other contributions to magnetization are small. Similar FC and ZFC magnetization curves as those in Fig. 9(b) were also reported for ordered $Sr_{0.5}La_{0.5}Ru_{0.5}Co_{0.5}O_3$ by Kim and Battle, although they did not associate such observation with the presence of $SrRuO_3$ clusters.[17]

In order to understand the magnetic behavior of the compounds at high temperatures, we have employed the Curie-Weiss analysis of the magnetization data (dc, at 1 T). The results showed that at temperatures $T > T_C$ susceptibility of all samples follows the Curie-Weiss law. The parameters θ_{CW} and μ_{eff} were extracted from the fits of 1 T FC magnetization data, and are tabulated in Table I. It is seen that the Curie-Weiss temperature continuously decreases with x, indicating a decrease in the strength of ferromagnetic interactions. This trend is consistent with the analysis of weak-field magnetization above. The effective magnetic moment, on the other hand, increases with the Co concentration. The increase is larger than the ones theoretically predicted for the various possible mixtures of Ru and Co ions: $Ru^{4+}(S=1)$ and high spin $Co^{3+}(S=2)$, $Ru^{5+}(S=3/2)$ and high spin $Co^{2+}(S=3/2)$, and their combination. The discrepancy could be due to induced magnetic moments around Co that survive to relatively high temperatures. The effective moments is also larger than the "saturation moment" per B-site μ_{sat}, calculated from the magnetization at 9 T and 10 K and listed in Table I, by a factor of 1.9 at $x=0$ and 5.7 at $x=0.3$. Theoretically, this ratio ($[(S+1)/S]^{1/2}$) should be 1.4 for $S=1$ if all magnetic moments are localized. The difference in the data of the ordered and disordered samples is too small to warrant a further interpretation.

E. Resistivity

The end members of the $Sr_{1-x}La_xRu_{1-x}Co_xO_3$ system are metallic $SrRuO_3$ and insulating $LaCoO_3$, which undergoes an insulator/metal transition at 500 K.[9,29] The resistivity of $Sr_{1-x}La_xRu_{1-x}Co_xO_3$ shown in Fig. 10 increases with x, but remains metallic at low x. For the ferromagnetic samples ($x=0$ and 0.1) a resistivity kink at T_c is present. Samples with $x>0.1$ do not show metallic behavior at $T<350$ K and their resistivity shows no feature at the magnetic transition temperatures. Such behavior is qualitatively similar to that of $Sr_{1-x}La_xRu_{1-x}Fe_xO_3$.[4] Also similar is the variable range hopping behavior for the samples with higher x, when the resistivity follows a $\rho(T)=\rho_0 \exp(T_0/T)^{1/4}$ dependence.[30] For the $x=0.4$ sample, this dependence is obeyed over ten orders of magnitude, as shown in the inset of Fig. 10 for conductivity ($\sigma = \rho^{-1}$). The resistivity extrapolated to 0 K diverges for the $x=0.3$ and 0.4 samples but not for others. These features are again similar to those seen in the $Sr_{1-x}La_xRu_{1-x}Fe_xO_3$ series. However, the resistivity is generally higher in the $Sr_{1-x}La_xRu_{1-x}Co_xO_3$ series, indicating Co substitution causes more disruption to the conductivity path of the Ru network.

starts from an unusually high temperature, about 150 K. Interestingly, this excess magnetization was also seen in the $x=0.5$ sample when it was ordered [Fig. 9(b)], but disappeared when the sample was disordered [Fig. 9(c)]. In the latter disordered case, a cusp-shaped ZFC magnetization again appears, indicating that it is a good spin glass. [We did verify that curves in Fig. 9(c) could be reverted to those of Fig. 9(b) by reannealing the disordered sample to reestablish order.][18] Similar behavior was seen for the $x=0.4$ sample (data not shown.)

We believe that the excess magnetization that emerges just below 150 K is due to $SrRuO_3$ nanoclusters, which have a T_c close to that of $SrRuO_3$(162.26 K).[29] Paradoxially, these clusters are the natural consequence of incomplete Ru:Co ordering. This is because the ordered state first consumes regions where the ratio of Ru to Co is close to one. As the excess cations are rejected from such ordered regions, the composition of the surrounding becomes rich in either Co or Ru, enhancing the probability of forming $SrRuO_3$ nanoclusters. The amount of these ferromagnetic clusters is probably very small, however, since in the ac susceptibility curve there
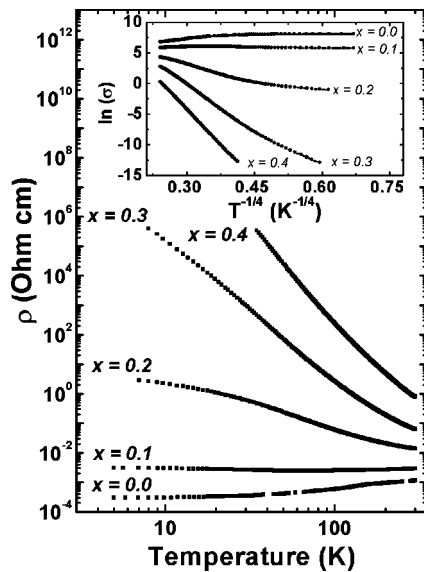
FIG. 10. Resistivity of $Sr_{1-x}La_xRu_{1-x}Co_xO_3$ as a function of temperature. Inset: conductivity plotted against $T^{1/4}$ showing variable range hopping in some samples.

It also indicates that mixed valence of Co^{2+}/Co^{3+} and Ru^{4+}/Ru^{5+} does not enhance conductivity in this system, therefore polaron transport is probably not the dominant conduction mechanism in the temperature range studied here.

For the $x=0.4$ sample, annealing at $1600°C$ followed by quenching caused a decrease in resistivity. Subsequent annealing at $1200°C$, however, did not result in further appreciable resistivity change. This suggests that the decrease in resistivity after $1600°C$ annealing is due to sintering and associated microstructure changes, and that long range ordering does not have a strong effect on conductivity.

F. Magnetoresistance

With the application of a magnetic field, the sample resistivity decreases, giving rise to a large negative magnetoresistace (MR) in some compositions. The temperature dependence of MR, measured at 9 T, was determined using disordered samples and shown in Fig. 11. Except for the x
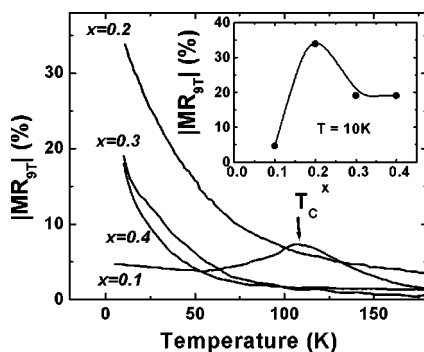

FIG. 11. Temperature dependence of negative magnetoresistance (MR) of $Sr_{1-x}La_xRu_{1-x}Co_xO_3$ samples, measured at 9 T. Negative MR is defined as $(\rho_0-\rho_H)/\rho_0$. Composition dependence at 10 K is shown in the inset.
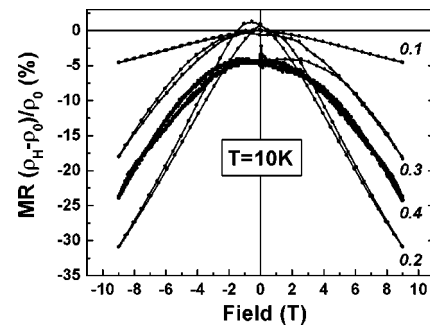

FIG. 12. Field dependence of the magnetoresistance (MR) of disordered $Sr_{1-x}La_xRu_{1-x}Co_xO_3$ samples, measured at 10 K, using field sweep from 0 T to 9 T to −9 T and back to 0 T. Data for $x=0.4$ are shifted down by 5% for clarity. The hysteresis is small in the ferromagnetic ($x=0.1$) sample, indicating little shape anisotropy. Hysteresis was more pronounced in other samples, but it always disappeared after the first complete field sweep.

$=0.1$ sample, there is a monotonic increase of MR with decreasing temperature, without any feature at the magnetic transition temperatures. Compared to other compositions, the MR is small for $x=0.1$ at low temperatures, but there is a peak at Tc. The composition dependence of MR, measured at 9 T and at 10 K, is shown in the inset.

We have further determined the field dependence of MR at 10 K. For such measurements we used a field sweep from 0 T to +9 T −9 T and back to 0 T, and recorded the resistance along the sweep. As illustrated in Fig. 12 for disordered samples, the MR at 10 K shows a symmetric field dependence. For small x, the curve is slightly concave downward. This changes to a nearly linear shape at larger $x(0.2)$ and finally slightly concave downward again at high $x(0.3$ and $0.4)$. The effect of ordering on MR proved to be rather small and is not shown in Fig. 12.

The above MR behavior is qualitatively similar to that of $Sr_{1-x}La_xRu_{1-x}Fe_xO_3$.. For a quantitative comparison, we plot in Fig. 13 the MR data at 10 K as a function of magnetization, in M^2, for several compositions. Also shown in dotted lines for comparison are data of $Sr_{1-x}La_xRu_{1-x}Fe_xO_3$ for $x=0.1,0.2,0.3,$ and 0.4. This plot indicates that at the same magnetization, the MR monotonically increases with x, and that the magnitude of MR is similar for $Sr_{1-x}La_xRu_{1-x}Co_xO_3$
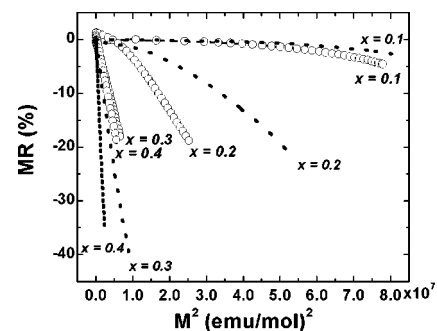

FIG. 13. Magnetoresistace (MR) of $Sr_{1-x}La_xRu_{1-x}Co_xO_3$ samples, measured at 9 T at 10 K as a function of magnetization, M^2. Also shown in dotted lines for comparison are the similar data of $Sr_{1-x}La_xRu_{1-x}Fe_xO_3$ for $x=0.1,0.2,0.3,$ and 0.4.

and $Sr_{1-x}La_xRu_{1-x}Fe_xO_3$ when compared at the same magnetization value. Note that the approximately linear M^2 dependence can be used to rationalize the shape of the different MR(H) curves observed in Fig. 12 once the shape of the nonferromagnetic portion of the hysteresis loops is taken into account.

IV. DISCUSSION

A. Cation charge states and electronic structures

We first summarize our findings in support of a charge transfer reaction from Ru^{4+}/Co^{3+} to Ru^{5+}/Co^{2+}. These are (a) direct evidence from XANES of Ru^{5+} structure, (b) B-site ordering indicating a large size and charge mismatch between Ru^{5+} and Co^{2+}, and (c) unit cell volume expansion of the intermediate composition at $x=0.5$(244.64 Å) over that of $SrRuO_3$(242.26 Å) and $LaCoO_3$(224.0 Å) and upon an increases of order. This reaction is apparently not reversible at low temperature, since we did not see any abrupt changes in the magnetic and transport properties during cooling indicative of a first-order transition associated with the reverse reaction. (It is first order in view of the volume change anticipated for the valence change.) This is unlike the case of $LaCoO_3$ in which $Co^{3+}(3d^6)$ is known to undergo several changes in the electronic configurations, from the low-spin state at low temperature, with the electronic configuration of (nonmagnetic) t_{2g}^6 and a smaller radius (0.545 Å), to an intermediate-spin state with the (magnetic) configuration $t_{2g}^5e_g^1$ (radius=0.56 Å) at temperatures between 100 and 500 K, to a final high-spin state with the (magnetic) configuration $t_{2g}^4e_g^2$ and a radius of 0.61 Å at above 600 K.[10] The presence of highly acidic Ru^{5+} is apparently more stabilizing for high-spin Co^{2+}, so it suppresses the various electronic transitions. Nevertheless, our XANES measurements showed that the Ru^{5+} state is more prominent when Ru and Co order on the B-site at higher Co concentrations. This suggests that Co−Co pairs would favor the trivalent state, and likewise Ru−Ru pairs would favor the tetravalent state. B-site ordering that maximizes Ru−Co pairing and minimizes Co−Co and Ru−Ru pairing, on the other hand, facilitates the charge transfer reaction.

The observed stability of Co^{2+} state in ruthenates and the XANES data allow us to construct an approximate electronic diagram for the Co^{3+} state in $SrRuO_3$. Here we use the same approach already applied to Fe^{3+} substitution in $SrRuO_3$ in **I**, i.e., we choose the top of the O 2p band as the reference level and assume that the energy of Ru (or Co) in $Sr_{1-x}La_xRu_{1-x}Co_xO_3$, relative to this reference level, is the same as in the end members ($SrRuO_3$ or $LaCoO_3$).[4] To further assign the energy levels of various bands, we also adopt the Zaalen-Sawazky-Allen model (ZSA) (Ref. 31) for parameters W, U, and Δ whose values are again extracted from the spectroscopic data of the end-member oxide compounds.[32] The schematic energy diagram for $Sr_{1-x}La_xRu_{1-x}Co_xO_3$ is shown in Fig. 14(a) which may be compared with a similar diagram for $Sr_{1-x}La_xRu_{1-x}Fe_xO_3$ in Fig. 14(b).[4] Here, the upper Hubbard band of Co^{3+} is located at $\Delta \sim 1$ eV above the O 2p band according to Arima et al.,[32] for the high-spin state

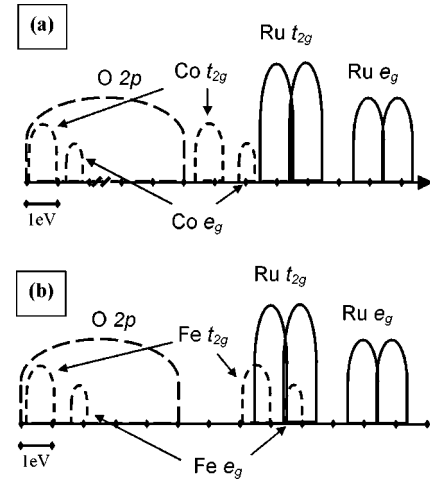FIG. 14. (a) Schematic energy levels of Ru^{4+} and Co^{3+} in $Sr_{1-x}La_xRu_{1-x}Co_xO_3$; (b) the same for Ru^{4+} and Fe^{3+} in $Sr_{1-x}La_xRu_{1-x}Fe_xO_3$, from **I** (Ref. 4). In constructing these diagrams, we used literature data (Ref. 32) to define the Zaanen-Sawatzky-Allen energies ($\Delta, U, 10$ Dq). In units of eV, they are (3,1.7,3) for Ru^{4+}, ($<1,7,1.3$) for Co^{3+}, and (2.6, 7, 1.3) for Fe^{3+}. We also let bandwidth W be 1 eV for all the t_{2g} and e_g bands.

($t_{2g\uparrow}^3e_{g\uparrow}^2t_{2g\downarrow}^1e_{g\downarrow}^0$ configuration). It is clear that the partially filled 3d levels of Co^{3+} in $SrRuO_3$ are well below the conduction band of Ru^{4+}. Therefore, it is energetically favorable to transfer electrons from the Ru^{4+} conduction band to the electronic states of Co, even though such electrons may become localized. The resulting Co^{2+} state would find the Δ to increase to ~ 2.4 eV (see Wei and Zi);[32] thus it is lifted to a level closer to, but still below, the Ru 4d levels.

This picture explains the fact the Co^{2+} is very stable in the presence of Ru^{5+}. In comparison with the 4d electrons, the 3d electrons of Co are more localized. Therefore, the formation of Co^{2+} occurs only when the Co ion has a neighboring Ru ion to donate an electron. Those Co ions surrounded by only Co ions have no charge transfer and stay in the Co^{3+} valence state.

B. Magnetism

The magnetic behavior of $Sr_{1-x}La_xRu_{1-x}Co_xO_3$ and $Sr_{1-x}La_xRu_{1-x}Fe_xO_3$ is rather similar, despite the formation of Ru^{5+} and Co^{2+} and the tendency for their ordering. Specifically, a similar phase diagram consisting of paramagnetic, ferromagnetic, cluster glass, and spin glass is observed, with similar transition temperatures, and a prominent enhancement of saturation magnetization is found at $x=0.1$. The main difference is that the phase boundaries appear to have shifted toward the lower x in the $Sr_{1-x}La_xRu_{1-x}Co_xO_3$ system, and that the saturation magnetization in the spin glass state is considerably higher in $Sr_{1-x}La_xRu_{1-x}Co_xO_3$ at large x. These similarities and differences reflect the general competition between the intinerant ferromagnetism of $SrRuO_3$ and the antiferromagnetic superexchange coupling between Co−Co (or Fe−Fe) pairs, further modified by the interaction between Ru and Co/Fe. The basis consequence of the above competition is the progressive destruction of itinerant ferro-

magnetism and the rise of a spin-glass state. In the case of $Sr_{1-x}La_xRu_{1-x}Co_xO_3$ the tendency for B-site Ru:Co ordering partially removes the antiferromagnetic contribution of Co–Co pairs, thus allowing a larger magnetization at x =0.4 and 0.5 than in $Sr_{1-x}La_xRu_{1-x}Fe_xO_3$. The enhancement of saturation magnetization at x=0.1 is believed to be caused by the ferromagnetic polarization of Ru electrons by Co/Fe magnetic cations, creating a large effective moment, since the bare moment of Co/Fe is too small to realign by a field at the field-temperature parameters observed. This effective moment is slightly lower in $Sr_{1-x}La_xRu_{1-x}Co_xO_3$ than in $Sr_{1-x}La_xRu_{1-x}Fe_xO_3$ judging from the slightly lower switching temperature at the same field (Fig. 5, inset). In the previous paper, we have argued that the peak composition of x=0.1 implies that the ferromagnetic Fe–Ru coupling is extended to the 6 first nearest neighbors but not yet to the 12 second nearest neighbors.[4] The same also holds in the case of Co–Ru coupling. This compares with the classical studies of Fe or Mn impurities in Pd, in which impurity-Pd interaction is believed to have extended to the second nearest neighbors.[3,33]

As described in **I**, the mechanism that is consistent with the ferromagnetic polarization by Fe^{3+} is the formation of a virtual bound state at the empty Fe $t_{2g}\downarrow$ state due to the resonance with the Ru $t_{2g}\downarrow$ electron at the Fermi level [see Fig. 14(b)]. This implies that the filled Ru $t_{2g}\downarrow$ subband is not participating, since it would have favored an antiferromagnetic coupling between the majority spins of Ru^{4+} and Fe^{3+}. For the same reason, the mechanism rules out the contribution of t_{2g} electrons from Ru^{5+}, which would also result in an antiferromagnetic coupling. (Indeed, the Ru^{5+}, compounds generally show semiconducting behavior and some antiferromagnetically order at low temperatures, e.g., Sr_2YRuO_6, $BaLaZnRuO_6$, and $Sr_3Ru_2O_7F_2$.[34–36]) It then follows that in $Sr_{1-x}La_xRu_{1-x}Co_xO_3$ the likely contribution to ferromagnetic polarization is by Co^{3+}/Ru^{4+} or Co^{2+}/Ru^{4+} resonance, in which the Ru $t_{2g}\downarrow$ electron forms a virtual bound state at the empty $Co^{2+}/Co^{3+}t_{2g}\downarrow$ state. (The Co^{2+} has one empty state while Co^{3+} has two empty states, so the final state population would favor Co^{3+}. On the other hand, Co^{2+} is closer in energy to Ru^{4+} than Co^{3+}, so the transition probability would favor Co^{2+}.) Since most likely there are several Ru^{4+} neighbors to each Co site in an octahedral environment, this polarization mechanism should be effective in $Sr_{1-x}La_xRu_{1-x}Co_xO_3$ despite the formation of Ru^{5+}, at least at x=0.1. Meanwhile, the formation of Ru^{5+} weakens itinerant ferromagnetism on one hand and disallows participation in the resonance mechanism on the other hand. This could explain the shift of phase boundaries toward the lower x and the slightly smaller induced magnetization at x=0.1 compared to the Fe substitution.

It is interesting to compare the effect of Fe and Co substitution with that of Mg and Ti, which are known to drastically decrease the magnetization at least at low fields. The latter data have been fitted with a $(1-x)^7$ dependence in the literature,[24,25] suggesting that the presence of merely one nearest (Mg/Ti) neighbor would destroy the magnetism of Ru. This is likely to be caused by charge localization, which should certainly cause the loss of itinerant ferromagnetism. Although there is definitely charge localization due to Fe and

Co substitution, the saturation magnetization can still increase at a high field. At low fields, Fe and Co substitution also decreased magnetization, but even at 0.01 T (less than those used in Refs. 24 and 25), we have found for 10% Fe and Co addition a much less reduction in remnant magnetization (about 30%) than that (50%) reported for Mg and Ti substitution. Therefore, the resonant scattering of Ru electrons at energetically similar Fe and Co states is clearly a very potent mechanism that negates the adverse effect of charge localization on itinerant magnetism.

C. Transport property and magnetoresistance

We first note that, for the temperature range studied here, $Sr_{1-x}La_xRu_{1-x}Co_xO_3$ is more resistive than $Sr_{1-x}La_xRu_{1-x}Fe_xO_3$ by a factor of 10–100 for compositions beyond x=0.1. This implies that Ru^{5+} and Co^{2+} contribute little to electronic conduction, i.e., the polaron mechanism is unimportant; instead, they deplete conduction electrons, promote localization, and increase scattering, presumably because of the more severe charge and size misfit associated with them. This is consistent with our proposed picture of electron conduction by mobile carriers whose energies lie beyond the mobility edge.[4] It is the spin polarization of these mobile carriers that is the origin of magnetoresistance.[4]

Just as in $Sr_{1-x}La_xRu_{1-x}Fe_xO_3$, a large negative magnetoresistance is observed in $Sr_{1-x}La_xRu_{1-x}Co_xO_3$ at the composition beyond the ferromagnetic regime. At 9 T, the maximum value of the MR in the $Sr_{1-x}La_xRu_{1-x}Co_xO_3$ occurs at about x=0.2 whereas in $Sr_{1-x}La_xRu_{1-x}Fe_xO_3$ it occurs near x=0.3. This peak is caused by the increasing difficulty in magnetizing the samples of higher Fe/Co content since, when compared at the same (nonferromagnetic) magnetization value, the MR at any given temperature. monotonically increases with x. The similar magnitude of MR in the two systems suggests a similar mechanism, with the relatively minor compositional shift caused by the charge-transfer reaction involving Co and Ru ions.

We have proposed in **I** a model that predicts that the MR of a random solid solution is initially of the order of $m^2/(1+m^2)$, were m is $M/M_{saturation}$. This would predict that the initial slope in Fig. 13 should be inversely proportional to $M^2/M_{saturation}$, which can be used to explain the trend in Fig. 13. For example, as the saturation magnetization in Fig. 6 monotonically decreases from x=0.01 to 0.3 the MR dependence on M^2 becomes stronger. Likewise, as $M_{saturation}$ becomes very similar for x=0.3 and 0.4 the M^2 dependence too becomes very similar. The above composition comparison applies to both Fe and Co systems. It also explains the relative magnitude of the slope when we compare MR $Sr_{1-x}La_xRu_{1-x}Fe_xO_3$ and $Sr_{1-x}La_xRu_{1-x}Co_xO_3$. For example, since the saturation magnetization is smaller in the Co substitutions than in the Fe substitutions for $x<0.3$ but the trend is reversed for $x>0.3$, the $MR-M^2$ dependence for $Sr_{1-x}La_xRu_{1-x}Co_xO_3$ is stronger in x=0.2, but weaker in x =0.3 and 0.4 than for $Sr_{1-x}La_xRu_{1-x}Fe_xO_3$. These favorable comparisons support our claim that the MR mechanism in these materials are the same and the model described in **I** is at least phenomenologically correct.

V. CONCLUSIONS

Unlike the $Sr_{1-x}La_xRu_{1-x}Fe_xO_3$ system (Ru^{4+}, Co^{3+}) in $Sr_{1-x}La_xRu_{1-x}Co_xO_3$ undergo a charge-transfer reaction to (Ru^{5+}, Co^{2+}) when they are nearest neighbors to each other. The large difference in size and charge between Ru^{5+} and Co^{2+} in turn motivates their ordering on the B-site sublattice. Meanwhile the resonance between Ru electrons and the energetically similar $Co^{2+}/Co^{3+} t_{2g}$ levels causes spin polarization and the formation of a large localized magnetic moment around Co. At higher Co and La concentrations, Anderson localization sets in, leaving relatively few mobile electrons at energy levels beyond the mobility edge. The population of these mobile electrons is biased by the spin polarization, thus allowing a large negative magnetoresistance. The common observations of large saturation magnetization and the negative magnetoresistance in both $LaFeO_3$ and $LaCoO_3$-substituted $SrRuO_3$, despite the complication of charge-transfer reactions and B-site ordering, provide an overall confirmation of the proposed picture for the effect of magnetic substitutional cations in conduction oxides.

APPENDIX

Weak field dc magnetization of $Sr_{0.8}La_{0.2}Ru_{0.8}Co_{0.2}O_3$ was examined to discern further evidence of spin glass, cluster glass, and ferromagnetic behavior. This composition features a strong frequency dependence in ac susceptibility, as shown in Fig. 8. Shown in Fig. 15(a) are the dc magnetization for the $x=0.2$ sample obtained under the (0.01 T) FC and ZFC conditions. These curves are different below T_c, suggesting a hysteretic behavior; however, the ZFC curve does not have a cusp shape characteristic of a spin glass. The
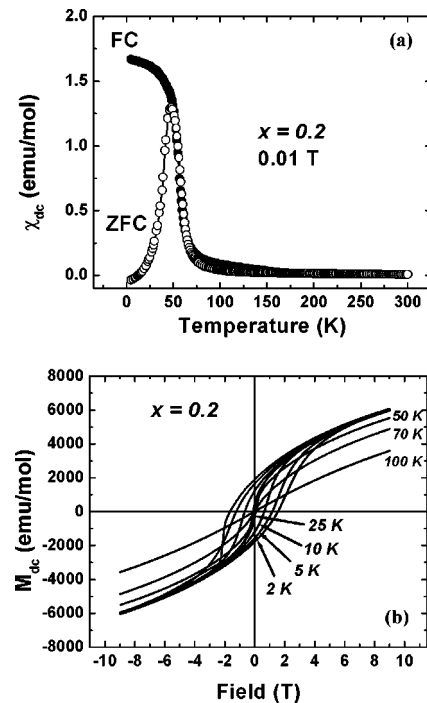

FIG. 15. Magnetic data of $Sr_{0.8}La_{0.2}Ru_{0.8}Co_{0.2}O_3$. (a) dc magnetization under (0.01 T) field-cooled (FC) and zero-field-cooled (ZFC) conditions. (b) *M-H* hysteresis curves at different temperatures.

reason for the different magnetization curves becomes apparent when we examine the *M-H* hysteresis curves, shown in Fig. 15(b) function of temperature. These hysteresis curves feature a relatively large coercive field compared to a "soft" ferromagnet. During the ZFC experiment, the sample was first cooled without a field, then a small field (0.01 T) was applied and the magnetization was measured on warming. Since the coercive field was large at low temperature, little magnetization could result until the temperature approached T_c when the coercive field decreases rapidly, giving rise to a sharp peak of ZFC magnetization. During the FC experiment, the magnetization was recorded during cooling under a small field (0.01 T). The induced magnetization obtained near T_c was then frozen at lower temperature because of coercivity. For the above reason, a large difference in the FC and ZFC magnetization becomes possible in the cluster glass composition.

*Corresponding author; Electronic address: iweichen@seas.upenn.edu

[1] On $SrRuO_3$ being a Stoner ferromagnet, see I. I. Mazin, and D. J. Singh, Phys. Rev. B **56**, 2556 (1997). On $SrRuO_3$ being a bad metal, see P. B. Allen, H. Berger, O. Chauvet, L. Forro, T. Jarlborg, A. Junod, B. Revaz, and G. Santi, *ibid.* **53**, 4393 (1996); L. Klein, J. S. Dodge, C. H. Ahn, G. J. Snyder, T. H. Geballe, M. R. Beasley, and A. Kapitulnik, Phys. Rev. Lett. **77**, 2774 (1996).

[2] A. M. Clogston, H. T. Matthias, M. Peter, H. J. Williams, E. Corenzwit, and R. C. Cherwook, Phys. Rev. **125**, 541 (1962).

[3] A. Oswald, R. Zeller, and P. H. Dederichs, Phys. Rev. Lett. **56**, 1419 (1986).

[4] A. Mamchik and I. W. Chen, preceding paper, Phys. Rev. B **70**, 104409 (2004).

[5] A. Mamchik and I. W. Chen, Appl. Phys. Lett. **82**, 613 (2003).

[6] P. W. Anderson, Phys. Rev. **124**, 41 (1961).

[7] P. A. Wolff, Phys. Rev. **124**, 1030 (1961)

[8] A. M. Clogston, Phys. Rev. **125**, 439 (1962).

[9] J. B. Goodenough, J. Phys. Chem. Solids **6**, 287 (1958).

[10] R. H. Potze, G. A. Sawatzky, and M. Abbate, Phys. Rev. B **51**, 11501 (1995).

[11] T. Saitoh, T. Mizokawa, A. Fujimori, M. Abbate, Y. Takeda, and M. Takano, Phys. Rev. B **55**, 4257 (1997).

[12] R. Caciuffo, D. Rinaldi, G. Barucca, J. Mira, J. Rivas, M. A. S. Rodriguez, P. G. Radaelli, D. Frorani, and J. B. Goodenough, Phys. Rev. B **59**, 1068 (1999).

[13] P. G. Radaelli and S.-W. Cheong, Phys. Rev. B **66**, 094408 (2002).

[14] L. Pi, A Maignan, R. Retoux, and B. Raveau, J. Phys.: Condens. Matter **14**, 7391 (2002).

[15] S. Manoharan, R. K. Sahu, D. Elefant, and C. M. Schneider, Solid State Commun. **125**, 103 (2003).

[16] B. Briceno, X-D Xiang, H. Chang, X. Sun, and P. G. Schultz, Science **270**, 273 (1995).

[17] S. H. Kim and P. D. Battle, J. Solid State Chem. **114**, 174 (1995).

[18] A. Mamchik, Ph.D. dissertation, University of Pennsylvania, Philadelphia, 2003.

[19] C. W. Jones, P. D. Battle, P. Lightfoot, and W. T. A. Harrison, Acta Crystallogr., Sect. C: Cryst. Struct. Commun. **45**, 365 (1989).

[20] H. Kobayashi, M. Nagata, R. Kanno, and Y. Kawamoto, Mater. Res. Bull. **29**, 1271 (1994).

[21] R. D. Shannon, Acta Crystallogr., Sect. A: Cryst. Phys., Diffr., Theor. Gen. Crystallogr. **32**, 751 (1976).

[22] P. D. Battle, T. C. Gibb, C. W. Jones, and F. Studer, J. Solid State Chem. **78**, 281 (1989).

[23] J. B. Goodenough, *Magnetism and the Chemical Bond* (Interscience, New York, 1963), p. 174.

[24] L. Mieville, T. H. Geballe, L. Antognazza, and K. Char, Appl. Phys. Lett. **70**, 126 (1997).

[25] D A. Crandles, Reedyk, R. W. Schaeffer, A. E. Hultgren, and R.

Schlee, Phys. Rev. B **65**, 224407 (2002).

[26] V. Jaccarino and L. R. Walker, Phys. Rev. Lett. **15**, 258 (1965).

[27] K. Binder and A. P. Young, Rev. Mod. Phys. **58**, 801 (1986).

[28] K. Moorjani and J. M. D. Coey, *Magnetic Glasses* (Elsevier, Amsterdam 1984), p. 301.

[29] D. Kim, B. L. Zink, F. Hellman, S. McCall, G. Cao, and J. E. Crow, Phys. Rev. B **67**, 100406 (2003).

[30] See, for example, A. L. Efros and M. Pollak, *Electron-Electron Interactions in Disordered Systems* (Elsevier, New York, 1985), pp. 297, 303, 432.

[31] J. Zaanen, G. A. Sawatzky, and J. W. Allen, Phys. Rev. Lett. **55**, 418 (1985).

[32] For Fe and Co, N. Hamada, H. Sawada, and K. Terakura, in *Spectroscopy of Mott Insulators and Correlated Metals*, edited by A. Fujmori and Y. Tokura (Springer-Verlag,Berlin, 1995), p. 95; T. Arima, Y. Tokura, and J. B. Torrance, Phys. Rev. B **48**, 17006 (1993); P. Wei, and Z. Q. Qi, *ibid.* **49**, 10864 (1994). For Ru: J. S. Lee, T. W. Noh, K. Char, J. Park, S.-J. Oh, J.-H. Park, C. B. Eom, T. Takeda, and R. Kanno, *ibid.* **64**, 245107 (2001); Y. S. Lee, J. S. Lee, T. W. Noh, D. Y. Byun, K. S. Yoo, K. Yamaura, and E. Takayama-Muromachi, cond-mat/0207012 v1, 30 June 2002.

[33] G. G. Low and T. M. Holden, Proc. Phys. Soc. London **89**, 119 (1966).

[34] G. Cao, Y. Xin, C. S. Alexander, and J. E. Crow, Phys. Rev. B **63**, 184432 (2001).

[35] I. Fernandez, R. Greatrex, and N. N. Greenwood, J. Solid State Chem. **32**, 97 (1980).

[36] R. K. Li and C. Greaves, Phys. Rev. B **62**, 3811 (2000).

[37] A. C. Larson and R. B. Von Dreele, Los Alamos National Laboratory Report, *General Structure Analysis System (GSAS)*; LAUR 86-748 (2000); B. H. Toby, J. Appl. Crystallogr. **34**, 210 (2001).